Bioactive Materials 41 (2024) 413–426

Contents lists available at ScienceDirect

Bioactive Materials

journal homepage: www.keaipublishing.com/en/journals/bioactive-materials

Camptothecin multifunctional nanoparticles effectively achieve a balance between the efficacy of breast cancer treatment and the preservation of intestinal homeostasis

Qingya Liu [a,1], Yun Yang [a,1], Meng Pan [a], Kun Shi [a], Dong Mo [a], Yicong Li [a], Meng Wang [a], Linfeng Guo [b], Zhiyong Qian [a,*]

[a] Department of Biotherapy, Cancer Center and State Key Laboratory of Biotherapy, West China Hospital, Sichuan University, Chengdu, 610041, China
[b] Department of Plastic and Burn Surgery, West China Hospital, Sichuan University, Chengdu, 610041, China

ARTICLE INFO

Keywords:
Camptothecin
PCRHNs
Intestinal barrier
Intestinal microbiota
Probiotics

ABSTRACT

Camptothecin (CPT) exhibits potent antitumor activity; however, its clinical application is limited by significant gastrointestinal adverse effects (GAEs). Although the severity of GAEs associated with CPT derivatives has decreased, the incidence rate of these adverse effects has remained high. CPT multifunctional nanoparticles (PCRHNs) have the potential to increase the efficacy of CPT while reducing side effects in major target organs; however, the impact of PCRHNs on the GAEs from CPT remains uncertain. Here, we investigated the therapeutic effects of PCRHNs and different doses of CPT and examined their impacts on the intestinal barrier and the intestinal microbiota. We found that the therapeutic efficacy of PCRHNs + Laser treatment was superior to that of high-dose CPT, and PCRHNs + Laser treatment also provided greater benefits by helping maintain intestinal barrier integrity, intestinal microbiota diversity, and intestinal microbiota abundance. In summary, compared to high-dose CPT treatment, PCRHNs + Laser treatment can effectively balance therapeutic effects and GAEs. A high dose of CPT promotes the enrichment of the pathogenic bacteria *Escherichia-Shigella*, which may be attributed to diarrhea caused by CPT, thus leading to a reduction in microbial burden; additionally, *Escherichia-Shigella* rapidly grows and occupies niches previously occupied by other bacteria that are lost due to diarrhea. PCRHNs + Laser treatment increased the abundance of *Lactobacillus* (probiotics), possibly due to the photothermal effect of the PCRHNs. This effect increased catalase activity, thus facilitating the conversion of hydrogen peroxide into oxygen within tumors and increasing oxygen levels in the body, which is conducive to the growth of facultative anaerobic bacteria.

1. Introduction

Camptothecin (CPT) is a potent chemotherapeutic agent that is active against various cancers, including breast cancer [1]. In the initial stages of clinical trials, CPT was formulated as a CPT sodium salt to achieve delicate equilibrium between its inactive carboxylate form (CPT-Na^+) and its active lactone form (CPT) at physiological pH. However, patients enrolled in these trials exhibited dose-dependent bone marrow suppression, hemorrhagic cystitis, and severe GAEs (including diarrhea, nausea, and vomiting), which led to the discontinuation of treatment [2,3]. It was not until the discovery of its unique antitumor mechanism, which inhibits DNA topoisomerase, that CPT regained prominence in antitumor research. Derivatives developed from the CPT structure, such as irinotecan and topotecan, have increased water solubility and mitigated associated GAEs. However, despite these improvements, the incidence of GAEs remains high [4,5], which significantly impacts patients' quality of life. Importantly, the antitumor activity of these derivatives is lower than that of CPT [6,7], which could compromise therapeutic efficacy and even jeopardize patients' lives.

Novel nanomedicine delivery systems utilize the properties of nanomaterials to enable excellent dispersibility of water-insoluble drugs in water, prolonged circulation time, tumor-targeting capability, and

Peer review under responsibility of KeAi Communications Co., Ltd.
* Corresponding author.
E-mail address: anderson-qian@163.com (Z. Qian).
[1] These authors contributed equally to this work.

https://doi.org/10.1016/j.bioactmat.2024.07.032
Received 12 June 2024; Received in revised form 27 July 2024; Accepted 27 July 2024

remarkable accumulation within tumors [8–11]. Furthermore, certain nanomaterials possess inherent characteristics such as photothermal and photodynamic effects, that can effectively enhance the efficacy of antitumor treatments [12–14]. These nanomaterial features offer promising opportunities to enhance the therapeutic efficacy of CPT while minimizing adverse effects. Over the past two decades, more than 15 nanomedicines have been approved for clinical use [15]. Furthermore, several CPT-based nanomedicines have progressed to clinical trials, with CPT-based antibody–drug conjugates (CPT-ADCs) being particularly noteworthy. However, achieving a formula that balances the three parts in the correct proportions is a challenge for scientists [16]. Combination therapy based on photothermal therapy has been designed to enhance the tumor targeting of CPT-ADCs, thereby effectively improving the efficacy of this tumor treatment and reducing potential side effects. In previous studies, our research group utilized the US Food and Drug Administration approved agent Prussian blue (PB) to design and synthesize PCRHNs for tumor targeting. The incorporation of the photothermal effect of PB enhances the antitumor efficacy of CPT, and this system mitigates adverse effects in vital organs [17]. However, the GAEs of CPT, which have been previously reported, were not investigated in this system. Considering the strong GAEs of CPT [2,3] and the fact that chemotherapy-induced GAEs may result in dose reduction, shortened treatment cycles, or even discontinuation of medication, which could lead to chemotherapy failure and pose a threat to patients' lives [18], it is necessary to study the GAEs of PCRHNs (See Scheme 1).

Numerous studies have shown that chemotherapy-induced GAEs are associated with alterations in the gastrointestinal microenvironment, where the intestinal barrier and microbiota play crucial roles [4,19–21]. The interaction between intestinal epithelial cells and tight junction proteins results in the formation of the intestinal barrier, which is crucial for maintaining intestinal homeostasis [22,23]. This barrier isolates the intestinal microbiota within the intestine, thereby preventing harmful substances from crossing and regulating intestinal permeability [24,25]. When chemotherapy drugs inhibit rapidly proliferating tumor cells, intestinal epithelial cells become vulnerable to attack by the drugs because of their short proliferation cycle and fast growth rate, resulting in intestinal injury [26]. The process mainly results in an increase in intestinal permeability and intestinal epithelial cell apoptosis and a decrease in intestinal tight junction proteins, resulting in chemotherapy-induced diarrhea [27].

Damage to the intestinal barrier often results in alterations in the composition of the intestinal microbiota [28]. The breakdown of food by the intestinal microbiota provides energy and nutrients for intestinal cells, while certain microorganisms in the intestine can increase chemotherapy sensitivity and alleviate adverse effects [29]. However, certain intestinal microorganisms have been implicated in the toxic side effects of chemotherapy [4]. Furthermore, chemotherapy agents can directly impact the intestinal microbiota and result in dysbiosis. This includes a decrease in intestinal microbial diversity and abundance, as well as a shift in microbial composition from more "beneficial" symbiotic microorganisms (such as *Bifidobacteria* and *Lactobacilli*) to more "pathogenic" microorganisms (including *Clostridium* and *Enterobacteriaceae*) [30]. Dysbiosis of the intestinal microbiota may contribute to mucositis, which exacerbates the clinical course of cancer [31].

The intestinal barrier and microbiota play important roles in human physiology and pathology, but the impact of chemotherapy drug nano materialization on these processes is still poorly understood. Building on prior research [17], we conducted a comparative study to evaluate the therapeutic effects of PCRHNs and different doses of free CPT, as well as their impact on intestinal barrier function and the microbiota. This

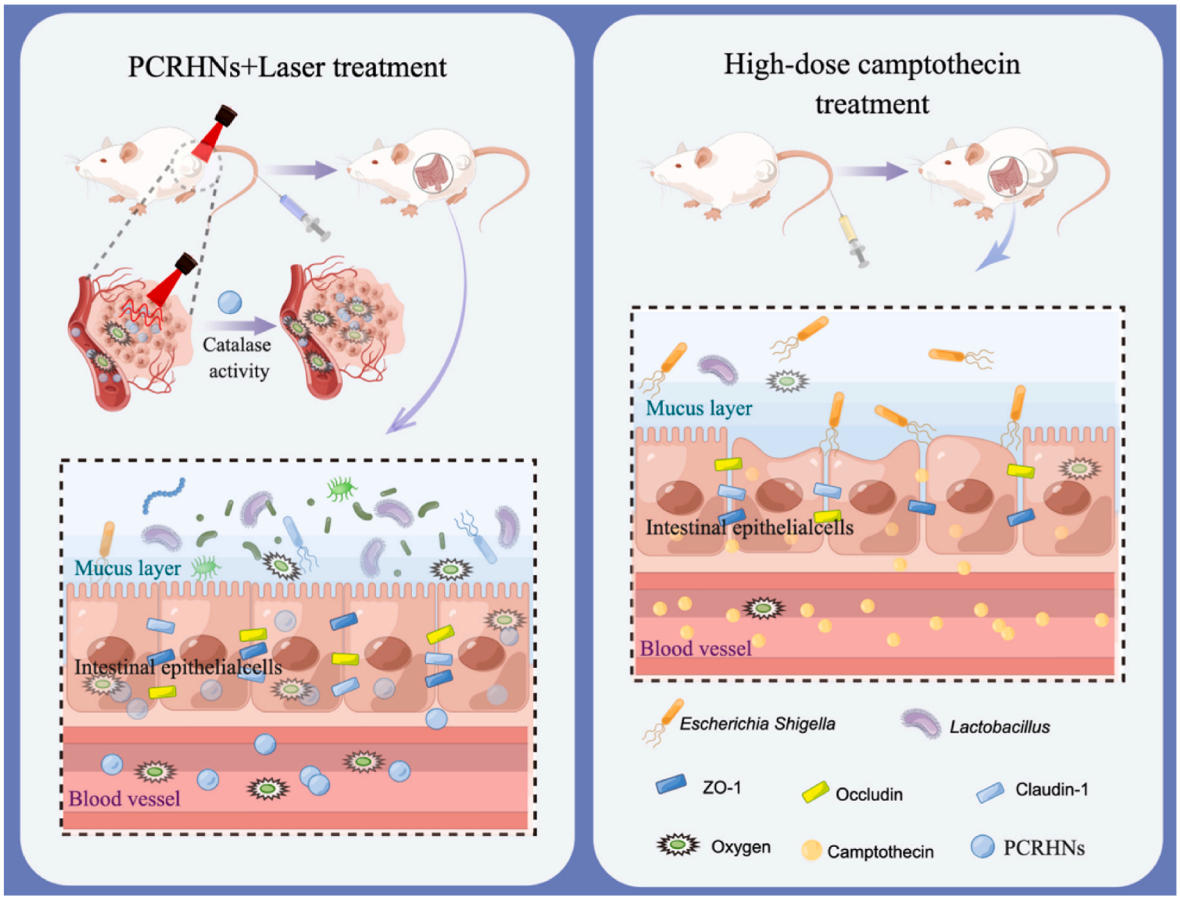

Scheme 1. Impact of PCRHNs + Laser treatment and high-dose CPT treatment on the intestinal barrier and microbiota. The drug enters the intestine from blood vessels and affects the integrity of the intestinal barrier and the composition of the intestinal microbiota.

investigation provides valuable insights into the impact of nanomedicines on GAEs, thereby establishing a foundation for assessing the safety of nanomedicines.

2. Methods

Preparation of PCRHNs: PB NPs and PCRHNs were prepared according to previously reported methods [17]. The particle size and polydispersity index (PDI) value of the PCRHNs were determined via a Malvern Zetasizer Nano ZS (Malvern Nano ZS 90, Malvern, UK), and their morphology was examined via transmission electron microscopy (TEM, Tecnai G2 F20 S-TWIN).

***In vitro* CPT release**: To evaluate the *in vitro* release of CPT from PCRHNs, 4.0 mg of PCRHNs were dispersed in 2.0 mL of PBS at pH 6.4 (containing 0 mmol/L glutathione (GSH) or 5.0 mmol/L GSH) and then transferred into dialysis bags (molecular weight cutoff: 3500 Da). A centrifuge tube was loaded with 20 mL of PBS (pH = 6.4), the dialysis bag was inserted into the tube, and the mixture was then placed on a shaker at 37 °C for agitation. At a designated time point, 2.0 ml of buffer solution was extracted from the test tube and replaced with an equal volume of fresh buffer solution. The CPT content was quantified via high-performance liquid chromatography (HPLC) using an Altima C18 analytical column and gradient elution of solvent A (CH_3CN containing 0.2 % acetic acid) and solvent B (H_2O containing 0.2 % acetic acid) at a flow rate of 1.0 mL/min, with the temperature maintained at 35 °C.

Photothermal performance of the PCRHNs: The increase in the temperature of the PCRHNs and PB NPs upon laser irradiation was investigated at a concentration of 0.5 mg/mL. PCRHNs and PB NPs solutions were irradiated with an 808 nm laser (Hi-Tech Opto-electronics Co., Ltd., Beijing, China) at a power density of 1.0 W/cm^2 for 5 min, and the temperature was recorded every minute. The laser irradiation stability of the PCRHNs was evaluated by subjecting the nanoparticles to 808 nm laser irradiation for five ON/OFF cycles, each lasting 5 min. The temperature was measured using a digital thermometer and a Fluke infrared thermal imaging system (Ti-32, Fluke).

Animals: Female BALB/c mice aged 5–6 weeks were procured from HFK Bioscience Co., Ltd. (Beijing, China) and housed under specific pathogen-free conditions with ad libitum access to standard chow and water. All animal procedures were approved by the West China Hospital, Sichuan University (Chengdu, P. R. China). The ethics approval number is 20220310025.

***In vivo* antitumor effects**: BALB/c mice were injected subcutaneously with 4T1 cells (1×10^6 per mouse). After reaching a tumor volume of approximately 100 mm^3, the mice were randomly divided into 6 groups of 5 mice each (saline, 2 mg/kg CPT, 5 mg/kg CPT, 8 mg/kg CPT, PCRHNs and PCRHNs + Laser). The dose of CPT administered to the PCRHNs was 2 mg/kg, which is consistent with previous studies [17]. For the PCRHNs + Laser treatment, 808 nm laser radiation at a power density of 1.5 W/cm^2 was applied to the tumors for 5 min at 6, 24, and 48 h after administration. The tumor volumes and body weights were assessed every other day. The tumor volume (mm^3) was calculated using the following formula: volume = length × width^2 × 0.5. The tumors were collected 18 days after administration and fixed in paraformaldehyde solution, after which tissue sections were prepared. Tumor proliferation was evaluated through immunohistochemical staining (Ki-67), and apoptosis was assessed using immunofluorescence staining (TUNEL). Immunohistochemical images were acquired using a 3DHISTECH Pannoramic (Pannoramic MIDI), and immunofluorescence-stained sections were analyzed using the AKOYA Vectra3 multispectral quantitative pathological analysis system.

***In vivo* intestinal permeability assay**: A 4T1 cancer model was established in female BALB/c mice. When the tumor volume reached 100 mm^3, the mice were divided into six groups ($n = 4$ for each group): saline, 2 mg/kg CPT, 5 mg/kg CPT, 8 mg/kg CPT, PCRHNs and PCRHNs + Laser. The morphology of the intestine was examined in mice on the fifth day after administration. The intestinal permeability of the mice was measured on the seventh day after treatment. After fasting for 4 h, the mice were administered FITC-dextran (440 mg/kg), and blood samples were collected 4 h later. The serum was separated from the blood, and the FITC-dextran concentration was measured using a fluorimeter with an excitation wavelength of 485 nm and an emission wavelength of 528 nm.

***In vitro* barrier assessment**: Caco-2 cells were seeded at a density of 1×10^5 in 6-well plates and allowed to proliferate for 72 h to establish Caco-2 monolayers. The cells were exposed to saline, 2 μg/mL CPT, 5 μg/mL CPT, 8 μg/mL CPT, or PCRHNs at a concentration of 20 μg/mL (with a CPT content of 10 %) for 24 h. The morphology of the Caco-2 cells was subsequently examined via light microscopy. In addition, Caco-2 cells were grown on glass cover slips to form Caco-2 monolayers and treated with saline, 2 μg/mL CPT, 5 μg/mL CPT, 8 μg/mL CPT, or PCRHNs at a concentration of 20 μg/mL (with a CPT content of 10 %) for 24 h. The cells were fixed with 4 % wt polyformaldehyde. Immunofluorescence staining was performed to label tight junction proteins using Bioss's ZO-1, Occludin, and Claudin-1 antibodies. The cells were imaged using a fluorescence microscope (Zeiss).

***In vivo* barrier assessment**: Colons were collected 7 days after drug administration and fixed in paraformaldehyde solution, after which tissue sections were prepared. Colon cell apoptosis was analyzed via immunohistochemical TUNEL staining, as previously reported [19]. To examine the distribution of tight junction proteins in the colon, tissue sections were immunostained with fluorescently labeled antibodies targeting ZO-1, Occludin, and Claudin-1. Immunohistochemical images were acquired using a 3DHISTECH Pannoramic (Pannoramic MIDI), and immunofluorescence-stained sections were analyzed using the AKOYA Vectra3 multispectral quantitative pathological analysis system.

Hematoxylin and eosin staining: The organs (heart, liver, spleen, lung, and kidney) from each group were fixed in 4 % paraformaldehyde for more than 24 h. After the organs were embedded in paraffin, they were sliced into thin sections and stained with hematoxylin and eosin (H&E). The sections were then evaluated using a 3DHISTECH Pannoramic system for pathological analysis.

Quantitative reverse transcription PCR: Total RNA was extracted from the colon samples using an E.Z.N.A. Kit I (Omega Biotek) according to the manufacturer's protocol. A cDNA reverse transcription kit (Yeasen, Shanghai, China) was used to perform reverse transcription. cDNA analysis was performed using SYBR Green qPCR Kits (Yeasen, Shanghai, China) on a CFX96 instrument (Bio-Rad). The cycling conditions were 95 °C for 2 min and 40 cycles of 95 °C for 10 s and 56 °C for 30 s. The relative expression of the target genes was determined via the use of GAPDH as a reference gene. The following primer sets were used for amplification: GAPDH-Fw, 5′-CATCAGTCCTTCCACGATACCA-3′; GAPDH-Rv, 5′-CCTGCACCACCAACTGCTTA-3′; ZO-1-Fw, 5′-CTTCTCTTGCTGGCCCTAAAC-3′; ZO-1-Rv, 5′-TGGCTTCACTTGAGGTTTCTG-3′; Occludin-Fw, 5′-CACACTTGCTTGGGACAGAG-3′; Occludin-Rv, 5′-TAGCCATAGCCTCC ATAGCC-3′; Claudin-1-Fw, 5′-ATGGCCAACGCGGGGCTG-3′; and Claudin-1-Rv, 5′-TTCCCACTAGAAGGTGTTGGC-3′.

Microbiota analysis: Fecal samples were collected 7 days after administration. DNA was extracted using an isolation kit (OMEGA Stool DNA Kit (50), D4015-01) according to the manufacturer's protocol. The extracted DNA was subsequently used to generate 16S rRNA libraries for community analysis via the MiSeq Illumina sequencing platform [32]. The V3–V4 region of the 16S rRNA gene was amplified using the primers 338F and 806R (338F, 5′-ACTCCTACGGGAGGCAGCA-3′; 806R, 5′-GGACTACHVGGGTWTCTAAT-3′) [19].

The operational taxonomic units (OTUs) were defined by applying a 97 % similarity threshold to all the data and subsequently clustered using QIIME2. The Shannon index and Chao1 index were used to evaluate alpha diversity. The Shannon index was used to quantify the diversity of the intestinal microbiota, whereas the Chao1 index was used to measure its abundance. Principal component analysis (PCA) was used to analyze the similarities and differences in the intestinal microbiota

among the different groups. Differences in the relative abundance of microbes were determined using linear discriminant analysis (LDA) effect size (LEfSe).

Inhibition of bacterial growth by CPT: Given the impact of high-dose CPT on the intestinal microbiota, we speculated that the effects may be due to the inhibition of strain proliferation by high doses of CPT. To investigate this hypothesis, we conducted an *in vitro* study to assess the impact of varying doses of CPT on the growth of *Shigella* sp., *Escherichia coli*, and *Lactobacillus reuteri*. Different concentrations of CPT were added to 20 mL of mixed medium (LB:TSA:MRAS = 1:1:1) and used to prepare different CPT solutions at concentrations of 2 μg/mL, 5 μg/mL, and 8 μg/mL and PCRHNs at a concentration of 20 μg/mL (with a CPT content of 10 %). A 1.5×10^8 CFU bacterial solution was added to each solution with different concentrations of CPT. After coculturing for 24 h, the bacteria were diluted and plated on Petri dishes to count the number of colonies (*Shigella* sp. was cultured in TSA, *E. coli* was cultured in LB, and *L. reuteri* was cultured with MRAS).

Determination of the bacterial growth rate: To determine the growth rates of the *Shigella* sp., *E. coli* and *L. reuteri* strains in mixed media, 1.5×10^8 CFU of each strain was added to 20 mL of mixed media. The mixture was then added to a 96-well plate, and the absorbance at 600 nm was measured every 2.5 h using an enzyme marker, after which a curve was generated.

Photoacoustic imaging *in vivo*: A 4T1 cancer model was established in BALB/c nude mice. When the tumor volume reached approximately 400 mm^3, the tumor-bearing mice were randomly divided into three groups (I: saline; II: PCRHNs; and III: PCRHNs + Laser group). Six hours after intravenous injection, the PCRHNs + Laser group was subjected to laser irradiation. A photoacoustic (PA) imaging system (inVision 128, iThera Medical GmbH, Neuherberg, Germany) was used to analyze Hboxygen signals from the mice.

Determination of oxygen production *in vitro*: The amount of oxygen generated by the PCRHNs and PCRHNs + Laser was measured at room temperature using a dissolved oxygen meter (JPB-608; Shanghai Instrument Electric Science instrument Limited by Share Ltd.) as previously described [33,34]. 200 μL of a 30 % hydrogen peroxide solution were added to 9.7 mL of PBS (pH 6.4), followed by the addition of 100 μL of PCRHNs (0.5 mg/mL) to the mixture. To investigate the impact of the laser on oxygen production, the above solution was irradiated with NIR for 10 min at a power density of 1.0 W/cm^2, after which oxygen production was measured. Moreover, the temperature changes in the solution were recorded. The effect of temperature on oxygen production was investigated in the same solution. The solution was placed in a water bath (IKA, Germany), in which the temperature was rapidly increased from 37 °C to 52 °C within 5 min. The oxygen content of the solution was continuously monitored throughout the heating process.

Statistical analysis: The data are presented as the mean ± standard error of the mean for results obtained from at least three independent trials. Statistical analyses were performed using Student's *t*-test and one-way ANOVA, and $p < 0.05$ was considered to indicate statistical significance ($^*p < 0.05$, $^{**}p < 0.01$, $^{***}p < 0.001$, and $^{****}p < 0.0001$). Statistical analysis was performed using GraphPad Prism software (version 9.0).

3. Results and discussion

3.1. Characterization of the PCRHNs

On the basis of our previous research, we prepared PCRHNs [17]. The average diameter of the PCRHNs was 164 ± 0.3 nm (Fig. 1A). Next, the morphology of the nanoparticles was investigated, as shown in Fig. 1B. The particle size and morphology of the PCRHNs were similar to those reported in previous research [17]. Additionally, the PCRHNs exhibited good stability. This findings was supported by the fact that even after being incubated in saline for several days, the PCRHNs did not show any signs of aggregation (Fig. S1), and there was only a minimal change in the PDI value (Fig. S2). The sensitivity of the nanoparticles to reducing conditions was verified by studying the release of CPT from the PCRHNs in the presence and absence of GSH. As shown in Fig. 1C, the release rate of CPT was slow in the absence of GSH. However, in the presence of GSH (5.0 mmol/L), CPT was released at a relatively rapid rate and reached 80 % release after 48 h. Many studies have shown that

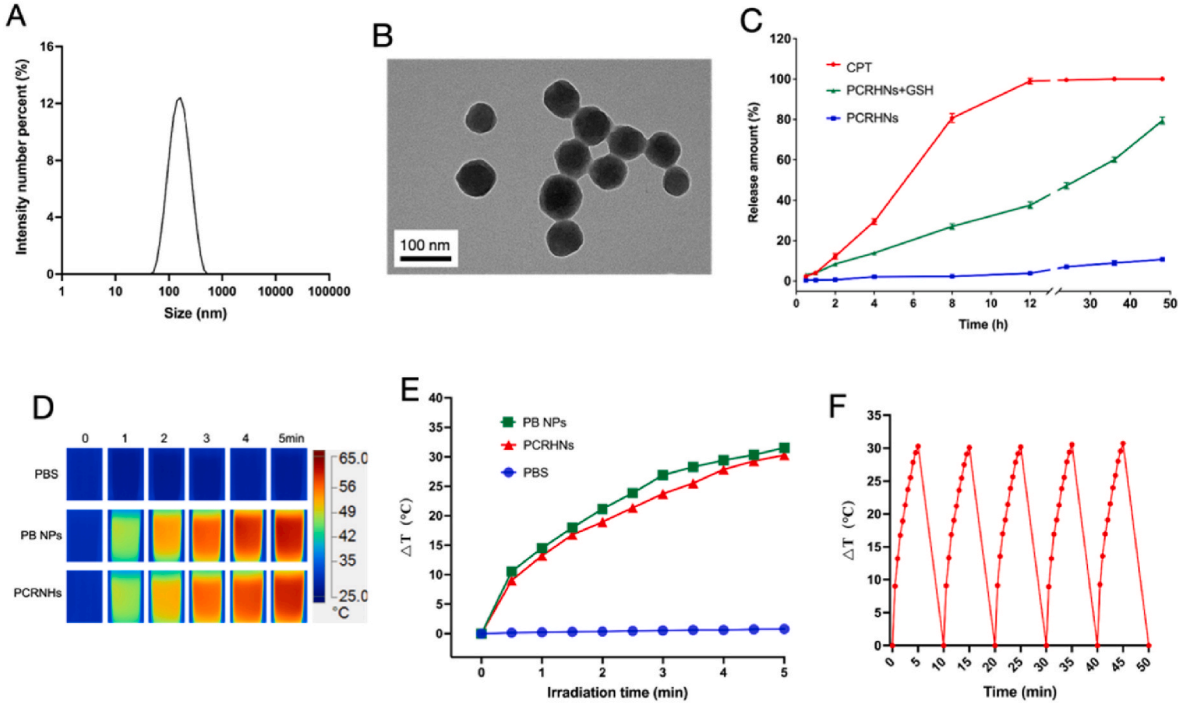

Fig. 1. Characterization of PCRHNs. Particle size (A) and TEM image (B) of PCRHNs. (C) *In vitro* CPT release profiles of PCRHNs at pH = 6.4. Infrared thermal images (D) and photothermal heating curves (E) of PCRHNs (0.5 mg/mL) under 808 nm laser irradiation at a power density of 1.0 W/cm^2 for 5 min. (F) Photothermal stability of PCRHNs under five cycles of irradiation.

the intracellular GSH concentration in tumor cells can reach 2–20 mM, which is 100–1000 times greater than that in the extracellular matrix and 7–10 times greater than that in normal tissues [14,35,36]. These results suggest that, compared with free CPT, PCRHNs exhibit a slower and more stable release rate while also demonstrating the ability to release CPT rapidly in response to GSH within tumor cells. The photothermal properties of the PCRHNs were subsequently examined. The infrared thermal images (Fig. 1D) and photothermal heating curves (Fig. 1E) revealed that there was no significant difference in the temperature increase between the PCRHNs and PB NPs when they were exposed to 808 nm laser irradiation. Moreover, even after undergoing five cycles of irradiation and cooling, the temperature of the PCRHNs remained consistent, indicating excellent photothermal stability (Fig. 1F). These findings were consistent with those of previous studies [17].

3.2. In vivo antitumor activity

The research indicates that there are challenges in balancing the effectiveness and toxicity of chemotherapy in the treatment of breast cancer [37]. Previous studies have shown that PCRHNs are effective in the treatment of breast cancer; however, limited research has been conducted on the incidence of GAEs from PCRHNs therapy [17]. This study aimed to compare the efficacy and GAEs of PCRHNs with high-dose CPT treatment, and the administration schedule is depicted in Fig. 2A. The results demonstrated that the therapeutic effects of 5 mg/kg and 8 mg/kg CPT were significantly better than those of 2 mg/kg CPT, indicating that free CPT inhibited tumor growth in a dose-dependent manner (Fig. 2B and C, Fig. S3). The dose-dependent inhibition of tumor growth by CPT was also demonstrated by observing tumor cell apoptosis (Fig. 2D) and proliferation (Fig. 2E). However, the therapeutic effects of the 5 mg/kg and 8 mg/kg CPT treatments were significantly

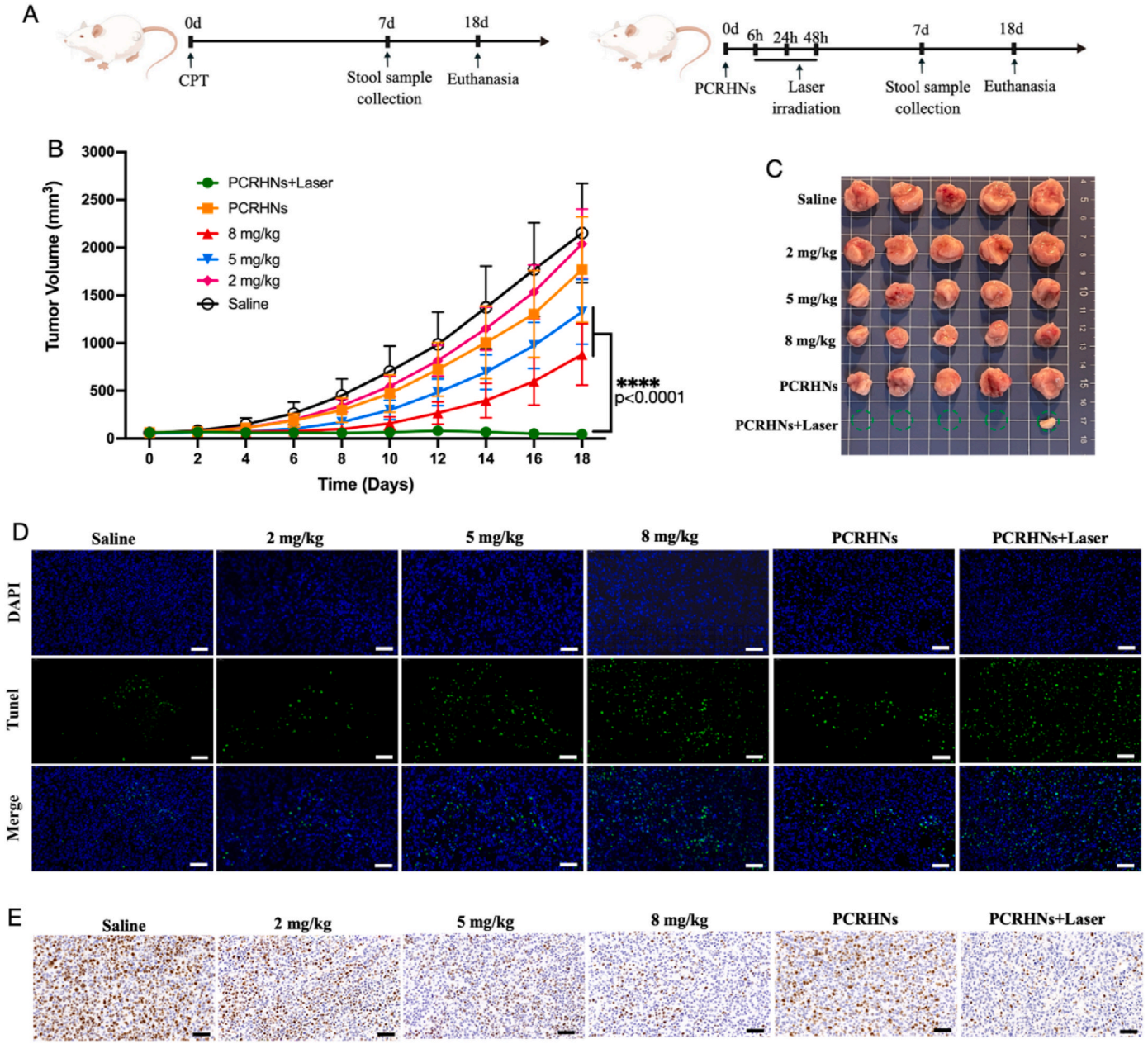

Fig. 2. Antitumor effects of PCRHNs + Laser therapy. (A) Administration schedule. (B) Tumor growth curves of the mice in each group were generated (****$P <$ 0.0001, analyzed by Student's *t*-test). (C) Images of the tumors were collected from the different groups after therapy. TUNEL (D) and Ki-67 (E) staining of tumors in each group. Scale bars, 50 μm.

inferior to those of the PCRHNs + Laser treatment group (with a CPT concentration of 2 mg/kg). Moreover, no noticeable alterations in tissue morphology or inflammatory cell infiltration were observed in H&E-stained sections of the heart, liver, spleen, lung, or kidney in the saline- or PCRHNs + Laser-treated groups (Fig. S4). These findings indicate that, compared with high-dose free CPT therapy, PCRHNs + Laser therapy can achieve superior therapeutic efficacy.

3.3. *In vitro and in vivo intestinal barrier*

On the basis of their antitumor efficacy, we investigated the effects of PCRHNs, PCRHNs + Laser therapy, and various doses of CPT on the intestinal barrier. The administration of increasing doses of CPT led to gradual loosening of the tightly connected Caco-2 cells and increasingly blurred cell boundaries. However, there was no significant difference in the morphology of Caco-2 cells between the group treated with PCRHNs and the saline group (Fig. 3A). Moreover, immunofluorescence staining of Caco-2 cells revealed that the levels of the tight junction proteins ZO-1 (Fig. 3B), Occludin (Fig. 3C), and Claudin-1 (Fig. 3D) decreased with increasing doses of CPT. However, there was no significant difference in the expression of these tight junction proteins between the PCRHNs-treated group and the saline group.

After evaluating the intestinal barrier *in vitro*, we proceeded to conduct an *in vivo* assessment of the intestinal barrier. First, we found that the percentage of weight loss in mice receiving a dose of 8 mg/kg was significantly greater than that in the other treatment groups from day 4 to day 8 of treatment (Fig. 4A). On the fifth day after administration, mice in the 8 mg/kg group exhibited fecal adhesion at the anus and the accumulation of a large amount of fluid in the cecum and colon, while no such phenomena were observed in the other groups (Fig. 4B). We subsequently conducted a study on intestinal permeability on the seventh day, which serves as an indicator of damage to the intestinal mucosa and is a crucial parameter for assessing the integrity of the intestinal barrier [38,39]. We found that PCRHNs + Laser therapy resulted in a significantly lower exposure to FITC-dextran in the blood vessels compared to free CPT therapy at doses of 8 mg/kg (Fig. 4C). The mice treated with 8 mg/kg of CPT exhibited the shortest colon length (Fig. 4D and E). Subsequently, we studied intestinal cell apoptosis to further assess the extent of intestinal injury among the different treatment groups. These findings suggest that the administration of high-dose CPT (5 mg/kg and 8 mg/kg) results in an increase in TUNEL-positive cells in the colonic epithelium compared with those in the other treatment groups (Fig. 4F). Research has demonstrated that the efficacy of tumor cell suppression is positively correlated with the dosage of the administered drug; however, higher dosages may give rise to off-target effects such as toxicity [40,41]. The present study demonstrated the occurrence of intestinal damage resulting from off-target effects induced by a high dosage of CPT.

Furthermore, we performed a comparative analysis of the distribution and expression of tight junction proteins in the colon. ZO-1, Occludin, and Claudin-1 are pivotal proteins that establish tight connections within the intestine and play crucial roles in maintaining intestinal homeostasis [42–44]. Immunofluorescence analysis revealed no significant differences in the protein levels of ZO-1 (Fig. 5A), Occludin (Fig. 5B) or Claudin-1 (Fig. 5C) among the PCRHNs, PCRHNs + Laser, and saline groups. However, these proteins were significantly lower in the intestines of the mice treated with high-dose free CPT (5 mg/kg and 8 mg/kg) than in those of the PCRHNs, PCRHNs + Laser, and saline groups. In addition, the expression patterns and mRNA levels of ZO-1, Occludin, and Claudin-1 were significantly greater in the PCRHNs + Laser group than in the high-dose CPT treatment group (Fig. 5D). These findings are consistent with those obtained from the immunofluorescence analysis.

These findings suggest that a high dose of CPT can increase intestinal permeability, induce intestinal epithelial cell apoptosis, and diminish the distribution and expression of tight junction proteins within the intestine, resulting in significant damage to intestinal tissue. Compared to high-dose CPT, PCRHNs + Laser therapy offers greater advantages in preserving the integrity of the intestinal barrier function.

3.4. *Modulation of the intestinal microbiota*

The findings from our previous research indicate that the impact of chemotherapy drugs on the intestinal microbiota varies depending on the dosage, and there may be a correlation between the intestinal microbiota and therapeutic outcomes [19]. In this study, we analyzed the composition of the intestinal microbiota in mice exposed to different treatments, and sequence data have been deposited in the National Center for Biotechnology Information (NCBI) Sequence Read Archive (SRA) database with the accession number PRJNA1136424. To assess the impact of various treatments on the intestinal microbiota, we utilized Bray–Curtis analysis to perform PCA based on the OTUs. The PCA results revealed significant differences in the intestinal microbiota among the mice treated with 8 mg/kg free CPT and the remaining groups (Fig. 6A). Afterward, we examined the diversity and abundance of the intestinal microbiota. Compared with those in the other groups, the diversity (Fig. 6B) and abundance (Fig. 6C) of the intestinal microbiota in the 8 mg/kg treatment group were significantly lower. The diversity of the intestinal microbiota was lower in the PCRHNs + Laser treatment group than in the PCRHNs group (Fig. 6B); however, there was no significant difference in abundance between the two groups (Fig. 6C). The diversity and abundance of the intestinal microbiota are reportedly associated with disease occurrence and treatment, and higher diversity and abundance may contribute to patient health [45,46].

Further analysis of the microbiota composition at the genus level revealed a significant increase in the abundance of *Escherichia-Shigella* in the 8 mg/kg CPT treatment group (Fig. 6D and E). This bacterium is capable of penetrating epithelial cells and inducing macrophages to release IL-1β, which further triggers intestinal inflammation [47,48]. The abundance of *Lactobacillus* decreased as the dosage of CPT increased. Surprisingly, the relative abundance of *Lactobacillus* was significantly lower in the PCRHNs group than in the PCRHNs + Laser group (Fig. 6D and F). *Lactobacillus* species are gram-positive, facultative anaerobic or microaerophilic bacteria widely used in various fields as probiotics [49–52]. LEfSe analysis was subsequently performed with an LDA score of 4 to identify significant biomarkers at the species level comparing the PCRHNs group and the PCRHNs + Laser treatment group. We found that *Lactobacillus reuteri* was a biomarker species enriched in the PCRHNs + Laser treatment group (Fig. 6G and H). This bacterium is a facultative anaerobic microorganism that promotes human health by combating infections, mitigating inflammation, enhancing immunity, and promoting intestinal homeostasis [53–55].

There was a significant difference in the intestinal microbiota between the 8 mg/kg treatment group and the other treatment groups, leading us to speculate whether high-dose CPT inhibited the growth of certain bacteria. To confirm this hypothesis, the effects of various concentrations of CPT on the bacteria *L. reuteri*, *E. coli*, and *Shigella* sp. were investigated through *in vitro* cocultivation with CPT solutions. There was no significant variation in the number of bacterial colonies observed when the same bacteria were exposed to PCRHNs or different concentrations of CPT (Fig. 7A and B). However, *L. reuteri* produced fewer colonies than *E. coli* and *Shigella* sp. at the same concentration of CPT. In light of the aforementioned findings, we hypothesized that the enrichment of *Escherichia-Shigella* in the intestinal microbiota of the mice in the 8 mg/kg treatment group could be attributed to the bacterial growth rate. Subsequently, the growth rates of these bacteria were measured, and the results revealed that the growth rates of *E. coli* and *Shigella* sp. were significantly faster than that those of *L. reuteri* (Fig. 7C).

Studies have shown that irinotecan, a derivative of CPT, can increase intestinal permeability and result in diarrhea [25]. Patients diagnosed with diarrheal irritable bowel syndrome typically exhibit enhanced colonic transit, diminished intestinal microbial diversity, and elevated

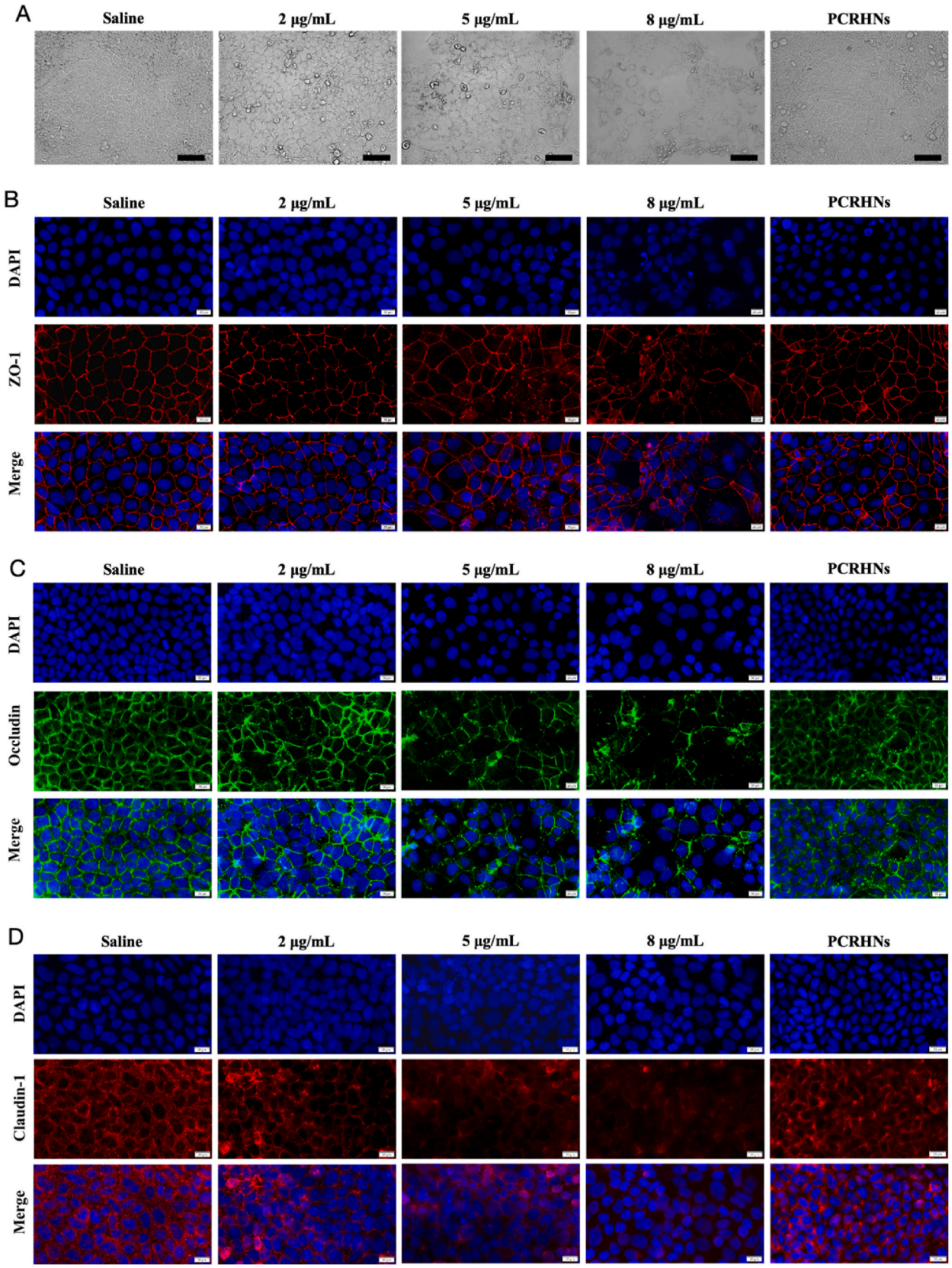

Fig. 3. *In vitro* barrier assessment. (A) Impact of PCRHNs (the concentration of PCRHNs was 20 μg/mL, with a CPT content of 10 %) and different doses of CPT on the morphology of Caco-2 cells (scale bar = 125 μm). Immunofluorescence staining analysis of ZO-1 (B), Occludin (C) and Claudin-1 (D) in the intestine (scale bar = 20 μm).

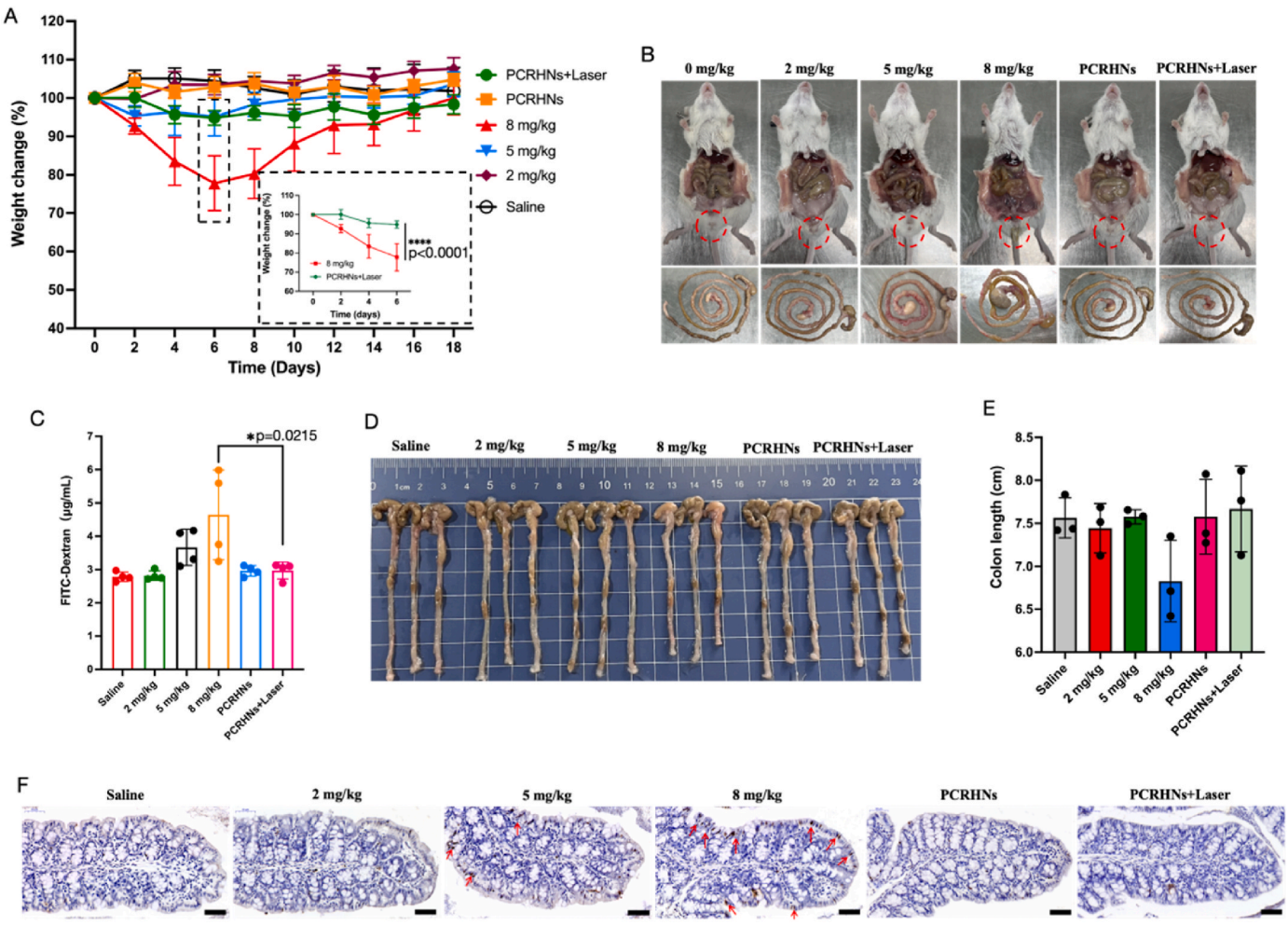

Fig. 4. PCRHNs + Laser therapy protects the colonic epithelium. (A) Changes in the body weights of the mice in the different treatment groups were determined (****$P < 0.0001$, analyzed by Student's *t*-test). (B) The adhesion status of mouse feces to the anus and the water content in the intestines were observed on the fifth day after administration. (C) Intestinal permeability was assessed in these mice by orally administering 4 kDa FITC-dextran on the seventh day after administration, followed by measuring the FITC-dextran signal in the blood (*$P < 0.05$, analyzed by Student's *t*-test). Images (D) and corresponding quantified lengths (E) of colons harvested from mice on the seventh day after different treatments. (F) TUNEL-positive epithelial cells indicate apoptosis in the colonic epithelium. Scale bars, 50 μm.

levels of *Enterobacteriaceae* [56]. In addition, Cheng et al. demonstrated that some supplemented bacteria were capable of occupying the niche previously occupied by members of the human gut microbiota [57]. In the present study, similar to the aforementioned report, we observed a significant increase in intestinal permeability in mice at a dosage of 8 mg/kg (Fig. 4C). This increase in permeability resulted in a substantial influx of fluid into the intestinal lumen (Fig. 4B), leading to the development of diarrhea in mice. Simultaneously, a high frequency of diarrhea resulted in reductions in both the diversity (Fig. 6B) and abundance (Fig. 6C) of the intestinal microbiota. Furthermore, enrichment of *Escherichia-Shigella* was observed in the 8 mg/kg treatment group in this study (Fig. 6D and E). On the basis of these experimental results and the effects of different doses of CPT on the *in vitro* growth of *L. reuteri*, *E. coli*, and *Shigella* sp., we suspect that high doses of CPT may trigger diarrhea while reducing the intestinal microbial load. Furthermore, the rapid proliferation of specific microorganisms (such as *Escherichia-Shigella*) may allow them to occupy ecological niches left vacant by other microorganisms.

In addition to variations in the intestinal microbiota induced by different doses of CPT, we also observed differences in the intestinal microbiota between the PCRHNs-treated group and the PCRHNs + Laser-treated group. The abundance of *Lactobacillus* in the PCRHNs + Laser group was significantly greater than that in the PCRHNs group (Fig. 6D–F, Fig. 6G), and these species are facultative anaerobic or microaerophilic bacteria widely used in various fields as probiotics [49–52]. It appears that PCRHNs + Laser treatment promotes the growth of facultative anaerobes and microaerophilic bacteria.

To validate this hypothesis, we conducted the experiment again to compare the effects of PCRHNs and PCRHNs + Laser treatment on the intestinal microbiota, and sequence data have been deposited in the SRA database with the accession number PRJNA1136405. Similar to the first experiment, the abundance of *Lactobacillus* in the PCRHNs + Laser group was significantly greater than that in the PCRHNs group (Fig. S5). LEfSe analysis revealed enrichment of *Lactobacillus taiwanensis*, *Acinetobacter towneri*, *L. reuteri*, *Staphylococcus succinus*, and *Actinobacillus capsulatus* in the PCRHNs + Laser group (Fig. S6). *L. taiwanensis* [58], *A. towneri* [59], *L. reuteri* [60], and *S. succinus* [61] are classified as facultative anaerobic bacteria, while *A. capsulatus* [62] is categorized as an aerobic bacterium. Notably, none of these bacteria are obligate anaerobes.

Intrigued by the enrichment of facultative anaerobic bacteria and aerobic bacteria in the PCRHNs + Laser group, we subsequently conducted an analysis to determine the underlying reasons for this phenomenon. Tumor tissues and cells exhibit significantly higher levels of hydrogen peroxide than their normal counterparts [63,64]. Moreover, PB NPs exhibit peroxidase activity at an optimal temperature of 50 °C for catalysis [65]. Research has shown that the colon's microecological environment is predominantly inhabited by obligate anaerobes [66]. Based on the above evidence, we suspect that laser irradiation induces

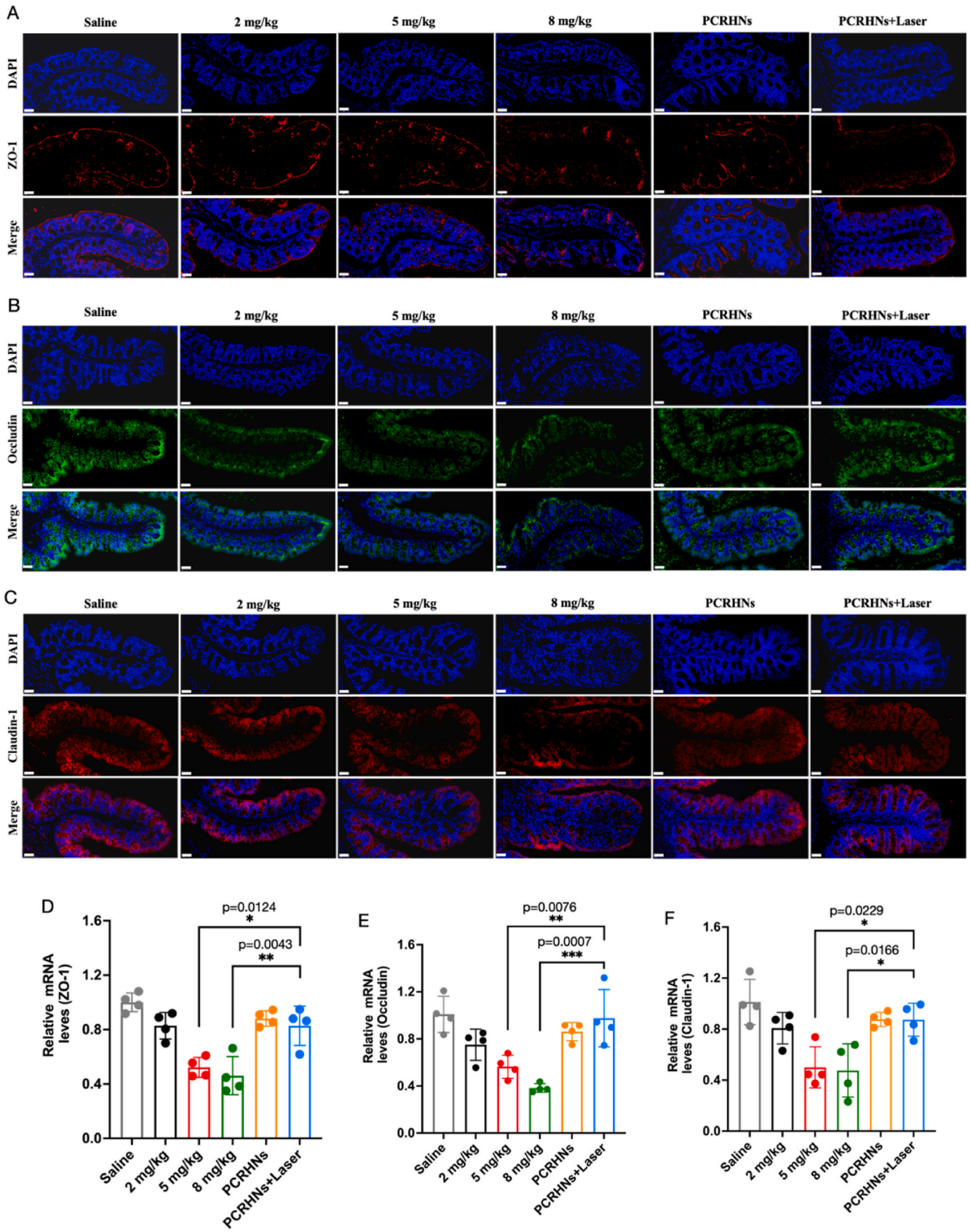

Fig. 5. PCRHNs + Laser treatment protects intestinal tight junction proteins. Immunofluorescence images of ZO-1 (A), Occludin (B) and Claudin-1 (C) staining in the colon. Scale bar, 50 μm. (D) ZO-1, Occludin and Claudin-1 mRNA levels in the colon (*$P < 0.05$, **$P < 0.01$, and ***$P < 0.001$; analyzed by one-way ANOVA).

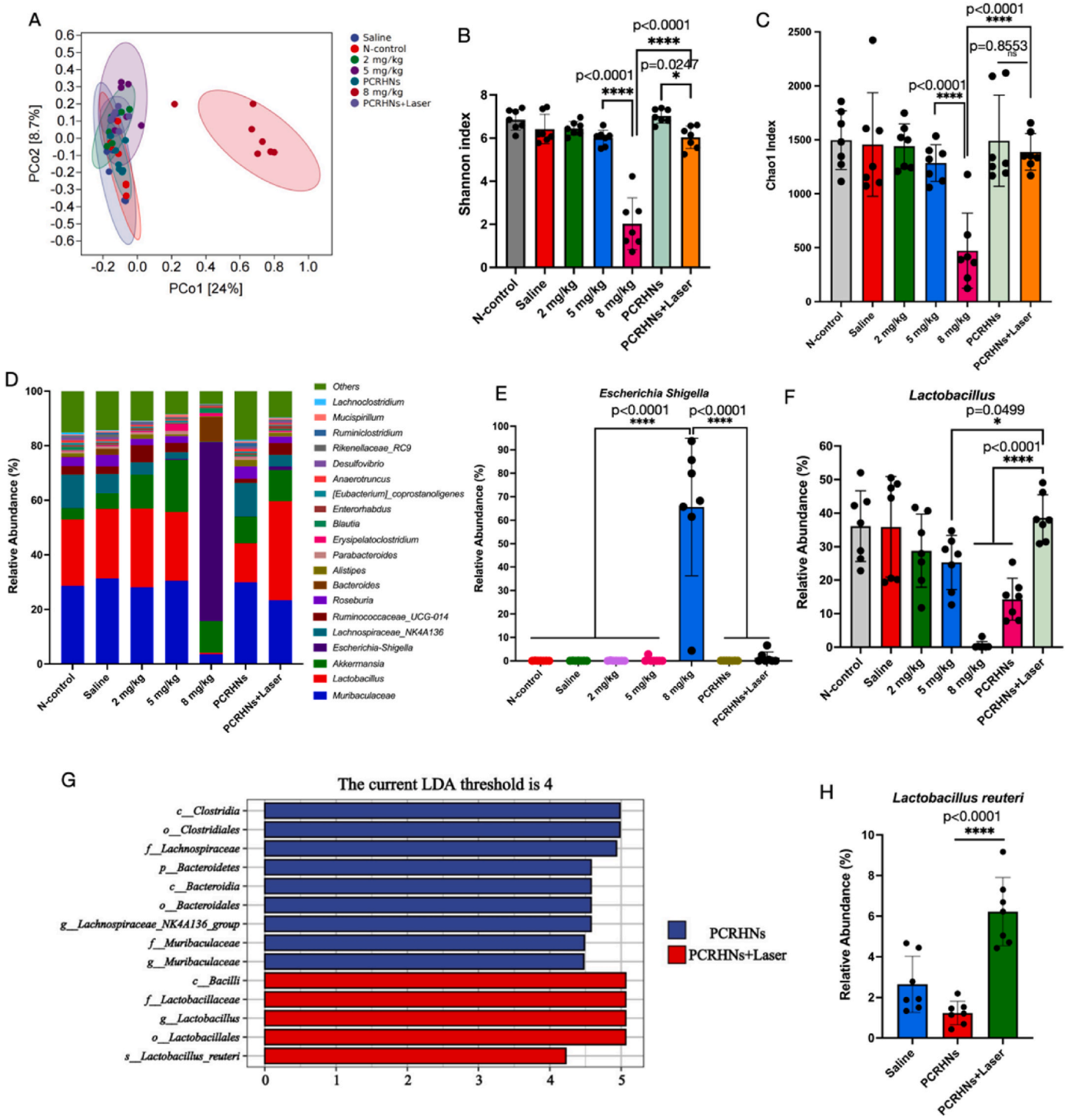

Fig. 6. PCRHNs + Laser therapy alters the composition of the intestinal microbiota. (A) PCA revealed the differences in the microbial communities among the samples. Each point represents one mouse. (B) Changes in the diversity of the intestinal microbiota are shown (Shannon index, $^{*}P < 0.05$ and $^{****}P < 0.0001$; analyzed by one-way ANOVA). (C) Changes in the abundance of the intestinal microbiota are shown (Chao1 index, $^{****}P < 0.0001$; analyzed by one-way ANOVA). (D) The composition and abundance of the intestinal microbiota at the genus level were determined. (E) The relative abundance of *Escherichia-Shigella* ($^{****}P < 0.0001$; analyzed by one-way ANOVA). (F) The relative abundance of *Lactobacillus* ($^{*}P < 0.05$ and $^{****}P < 0.0001$; analyzed by one-way ANOVA). (G) LEfSe histograms were generated. Bacterial taxa that met the criterion of an LDA score >4 were considered biomarker taxa. (H) The relative abundance of *Lactobacillus reuteri* ($^{****}P < 0.0001$; analyzed by one-way ANOVA).

localized hyperthermia at the tumor site, thereby accelerating the conversion of hydrogen peroxide to oxygen and increasing systemic oxygen levels. This ultimately promotes both facultative anaerobic bacteria and aerobic bacterial growth.

To validate this hypothesis, we conducted pertinent *in vivo* and *in vitro* experiments. Oxygen can convert deoxygenated hemoglobin into oxygenated hemoglobin (HbO_2) [33,67]. We evaluated the HbO_2 value of the tumors and found that it was significantly greater in the PCRHNs + Laser group than in the PCRHNs group (Fig. 8A and B). We subsequently conducted an *in vitro* study on oxygen production in the PCRHNs

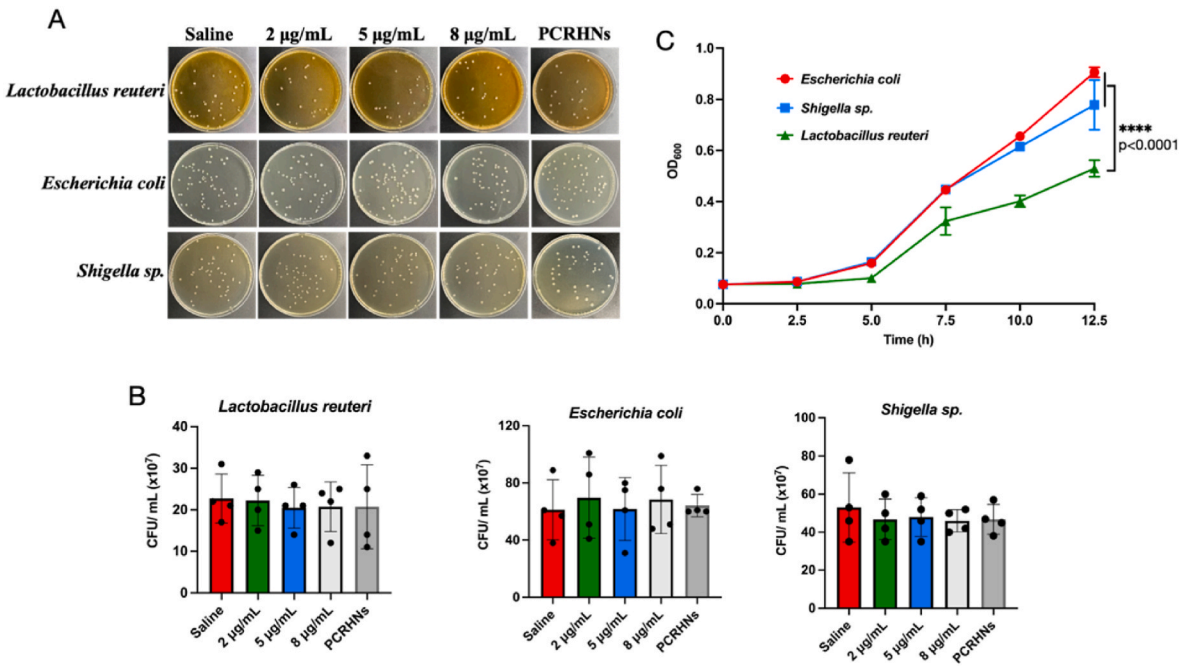

Fig. 7. The impact of PCRHNs and varying doses of CPT on bacterial proliferation. Representative images of viable colonies on suitable agar plates were taken after treatment with PCRHNs (the concentration of PCRHNs was 20 μg/mL, with a CPT content of 10 %) and various concentrations of CPT (A), and bacterial colony counting (B) was performed. (C) The absorbance of the biomass of *L. reuteri*, *E. coli* and *Shigella* sp. was measured at a wavelength of 600 nm (****$P < 0.0001$, analyzed by one-way ANOVA).

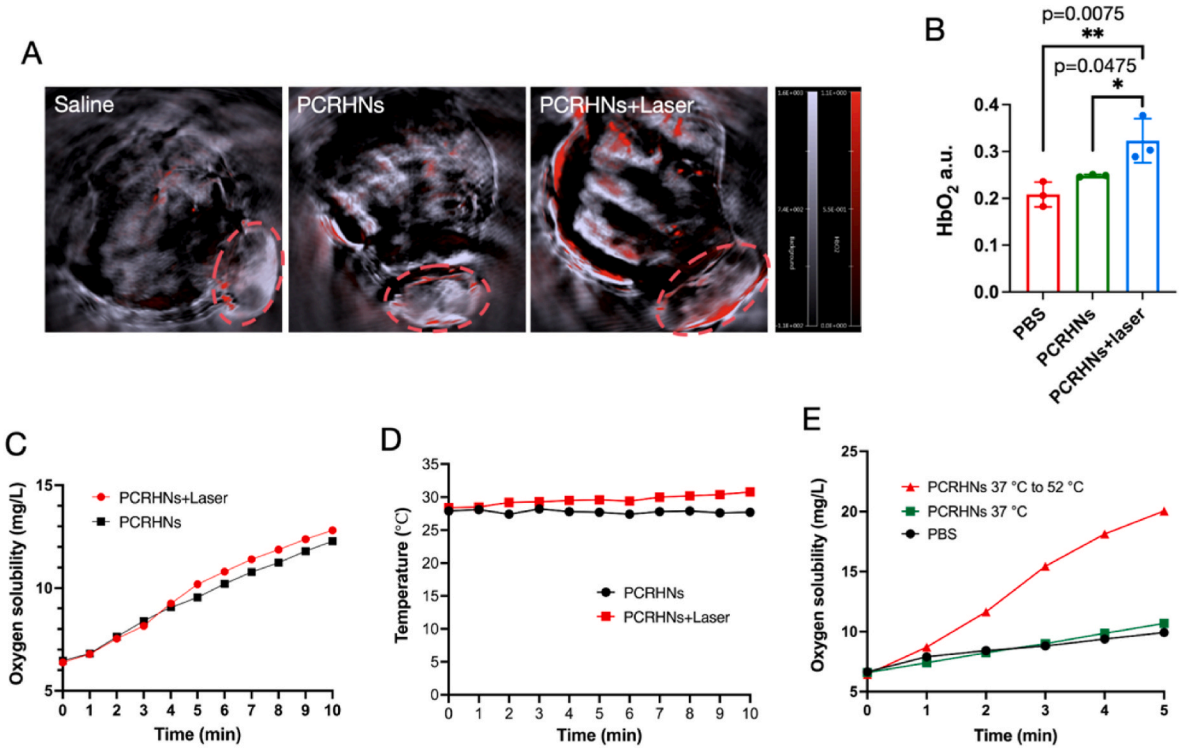

Fig. 8. Oxygen generation *in vitro* and *in vivo*. (A) PA images and (B) PA intensity were used to evaluate HbO_2 levels in 4T1 tumor-bearing mice (*$P < 0.05$ and **$P < 0.01$; analyzed by one-way ANOVA). In the PCRHNs + Laser group, PA images were obtained immediately after 5 min of laser irradiation (1.5 W/cm^2). (C) Oxygen generation and (D) temperature variation were measured. *In vitro*, the generation of oxygen from hydrogen peroxide was catalyzed by PCRHNs (0.005 mg/mL), and the temperature changed during the process. The laser irradiation intensity for the PCRHNs + Laser group was 1.0 W/cm^2, and the duration of exposure was 10 min. (E) PCRHNs catalyze the generation of oxygen from hydrogen peroxide as the temperature gradually increases from 37 °C to 52 °C.

and PCRHNs + Laser groups while simultaneously monitoring temperature fluctuations throughout the process. We found that there was no significant difference in oxygen production between the PCRHNs and PCRHNs + Laser groups at ambient temperature (Fig. 8C), and no significant variation in temperature was observed during this process (Fig. 8D). Previous research conducted by our group found that a solution of PCRHNs at a concentration of 0.02 mg/mL did not undergo noticeable heating upon laser irradiation [17]. In this study, no significant temperature change was observed in the PCRHNs + Laser group (PCRHNs concentration of 0.005 mg/mL) during *in vitro* oxygen production, which could be attributed to the low concentration of PCRHNs. As the tumor temperature of the mice in the PCRHNs + Laser group rapidly increased to 52.8 °C after 5 min of NIR laser irradiation [17], we simulated this process *in vitro* by gradually increasing the temperature of the system in a water bath and monitoring oxygen production during this process. Notably, in the presence of PCRHNs, oxygen production increased rapidly as heating progressed (Fig. 8E). These findings are consistent with previous reports, which indicate that the optimal temperature for determining the catalase activity of PB NPs is 50 °C [65].

These studies revealed that *Lactobacillus* was enriched in the PCRHNs + Laser group, potentially because of rapid laser irradiation-induced heating of the tumor site. This led to an increase in catalase activity, resulting in an increase in the conversion of hydrogen peroxide into oxygen within the tumor through catalysis and ultimately leading to an overall increase in the oxygen content. These factors are conducive to the proliferation of facultative anaerobic (such as *Lactobacillus*) and aerobic bacteria.

4. Conclusion

The results of this study demonstrate that, compared with high-dose free CPT, PCRHNs + Laser treatment effectively achieves a balance between therapeutic efficacy for breast cancer and low GAEs. High-dose free CPT leads to significant intestinal injury characterized by increased intestinal permeability, intestinal epithelial cell apoptosis, and a reduction in the level of tight junction proteins. In addition, the administration of high-dose CPT results in a dysregulated microbiota, which is characterized by reduced microbial diversity and abundance, as well as an increase in pathogenic bacteria (e.g., *Escherichia-Shigella*). This phenomenon may be attributed to the rapid proliferation of pathogens, which swiftly colonize the ecological niche vacated by other bacteria as a result of chemotherapy-induced diarrhea. Achieving both excellent therapeutic effects and few GAEs via free CPT treatment is challenging. However, the PCRHNs designed and synthesized by our research group effectively balance the antitumor effects and gastrointestinal-related toxicity. The efficacy of PCRHNs + Laser treatment is significantly superior to that of high-dose CPT, and the negative effects on the intestinal barrier and microbiota caused by high-dose CPT can be avoided. In addition, PCRHNs + Laser treatment promoted the proliferation of *Lactobacillus* (probiotics), possibly through the photothermal effect of the PCRHNs, which increased their catalase activity. This increase in activity accelerates the conversion of hydrogen peroxide into oxygen and increases oxygen levels in the body, which is conducive to the growth of facultative anaerobic bacteria that can grow with or without oxygen.

Ethics approval and consent to participate

All animal procedures were approved by the West China Hospital, Sichuan University (Chengdu, P. R. China). The ethics approval number is 20220310025.

CRediT authorship contribution statement

Qingya Liu: Writing – original draft, Software, Project administration, Methodology, Funding acquisition, Conceptualization. **Yun Yang:** Supervision, Methodology, Funding acquisition, Formal analysis, Data curation. **Meng Pan:** Validation, Software, Methodology. **Kun Shi:** Validation, Supervision, Methodology. **Dong Mo:** Visualization, Software, Methodology. **Yicong Li:** Visualization, Software, Methodology. **Meng Wang:** Methodology, Data curation. **Linfeng Guo:** Methodology. **Zhiyong Qian:** Supervision, Project administration, Methodology, Funding acquisition, Conceptualization.

Declaration of competing interest

Zhiyong Qian is an editorial board member for Bioactive Materials and was not involved in the editorial review or the decision to publish this article. All authors declare that there are no competing interests. The authors declare that they have no known competing financial interests or personal relationships that could have appeared to influence the work reported in this paper.

Acknowledgements

This work was funded by the National Natural Science Foundation of China Regional Innovation and Development Joint Fund (NSFCU21A20417), the National Natural Science Foundation of China (NSFC31930067, NSFC32001003, NSFC82202320), the Natural Science Foundation of Sichuan Province (2022NSFSC1282), and the 135 Project for Disciplines of Excellence, West China Hospital, Sichuan University (ZYGD18002). We also thank the support by Post-Doctor Research Project, West China Hospital, Sichuan University (2023HXBH011, 19HXBH099), Postdoctoral Interdisciplinary Innovation Foundation Project of Sichuan University (1082204112G23), China Postdoctoral Science Foundation (2023M742476) and the Natural Science Foundation of Sichuan Province (2023NSFSC1585).

Appendix A. Supplementary data

Supplementary data to this article can be found online at https://doi.org/10.1016/j.bioactmat.2024.07.032.

References

[1] Z.R. Wang, N. Little, J.W. Chen, K.T. Lambesis, K.T. Le, W.G. Han, A.J. Scott, J. Q. Lu, Immunogenic camptothesome nanovesicles comprising sphingomyelin-derived camptothecin bilayers for safe and synergistic cancer immunochemotherapy, Nat. Nanotechnol. 16 (2021) 1130–1140, https://doi.org/10.1038/s41565-021-00950-z.

[2] N.N.T. Quynh, K.X.T. Trinh, N.T. Trinh, V.T. Vo, N. Li, Y. Nagasaki, L.B. Vong, A silica-based antioxidant nanoparticle for oral delivery of Camptothecin which reduces intestinal side effects while improving drug efficacy for colon cancer treatment, Acta Biomater. 15 (2022) 459–470, https://doi.org/10.1016/j.actbio.2022.02.036.

[3] Y. Pommier, Topoisomerase I inhibitors: camptothecins and beyond, Nat. Rev. Cancer 6 (2006) 789–802, https://doi.org/10.1038/nrc1977.

[4] A.N. Chamseddine, M. Ducreux, J.P. Armand, X. Paoletti, T. Satar, A. Paci, O. Mir, Intestinal bacterial β-glucuronidase as a possible predictive biomarker of irinotecan-induced diarrhea severity, Pharmacol. Ther. 199 (2019) 1–15, https://doi.org/10.1016/j.pharmthera.2019.03.002.

[5] N. Baize, I. Monnet, L. Greillier, M. Geier, H. Lena, H. Janicot, A. Vergnenegre, J. Crequit, R. Lamy, J.B. Auliac, J. Letreut, H. Le Caer, R. Gervais, E. Dansin, A. Madroszyk, P.A. Renault, G. Le Garff, L. Falchero, H. Berard, R. Schott, P. Saulnier, C. Chouaid, Carboplatin plus etoposide versus topotecan as second-line treatment for patients with sensitive relapsed small-cell lung cancer: an open-label, multicentre, randomised, phase 3 trial, Lancet Oncol. 21 (2020) 1224–1233, https://doi.org/10.1016/S1470-2045(20)30461-7.

[6] H.A. Burris 3rd, A.R. Hanauske, R.K. Johnson, M.H. Marshall, J.G. Kuhn, S. G. Hilsenbeck, D.D. Von Hoff, Activity of topotecan, a new topoisomerase I inhibitor, against human tumor colony-forming units in vitro, J. Natl. Cancer Inst. 84 (1992) 1816–1820, https://doi.org/10.1093/jnci/84.23.1816.

[7] R.P. Hertzberg, M.J. Caranfa, K.G. Holden, D.R. Jakas, G. Gallagher, M.R. Mattern, S.M. Mong, J.O. Bartus, R.K. Johnson, W.D. Kingsbury, Modification of the hydroxy lactone ring of camptothecin: inhibition of mammalian topoisomerase I and biological activity, J. Med. Chem. 32 (1989) 715–720, https://doi.org/10.1021/jm00123a038.

[8] Z. Pei, H. Lei, L. Cheng, Bioactive inorganic nanomaterials for cancer theranostics, Chem. Soc. Rev. 52 (2023) 2031–2081, https://doi.org/10.1039/d2cs00352j.

[9] R. Liu, C. Luo, Z.Q. Pang, J.M. Zhang, S.B. Ruan, M.Y. Wu, L. Wang, T. Sun, N. Li, L. Han, J.J. Shi, Y.Y. Huang, W.S. Guo, S.J. Peng, W.H. Zhou, H.L. Gao, Advances of Nanoparticles as Drug Delivery Systems for Disease Diagnosis and Treatment, vol. 34, 2023 107518, https://doi.org/10.1016/j.cclet.2022.05.032.
[10] C.S. Huang, Q.C. Xu, C. Dai, L. Wang, Y.C. Tien, F. Li, Q. Su, X.T. Huang, J. Wu, W. Zhao, X.Y. Yin, Nanomaterial-facilitated cyclin-dependent kinase 7 inhibition suppresses gallbladder cancer progression via targeting transcriptional addiction, ACS Nano 15 (2021) 14744–14755, https://doi.org/10.1021/acsnano.1c04570.
[11] W. Chen, K. Shi, Y. Yu, P.P. Yang, Z.W. Bei, D. Mo, L.P. Yuan, M. Pan, Y. Chen, Z. Y. Qian, Drug delivery systems for colorectal cancer chemotherapy, Chin. Chem. Lett. 35 (2024) 109159, https://doi.org/10.1016/j.cclet.2023.109159.
[12] Y. Zhu, Y.Q. Wu, S.S. Li, X.L. Yuan, J. Shen, S.Y. Luo, Z.S. Wang, R. Gao, J. Wu, L. Ge, Photocatalytic and photothermal bismuthene nanosheets as drug carrier capable of generating CO to improve drug sensitivity and reduce inflammation for enhanced cancer therapy, Chem. Eng. J. 446 (2022) 137321, https://doi.org/10.1016/j.cej.2022.137321.
[13] Y. Yang, Q.Y. Liu, M. Wang, L. Li, Y. Yu, M. Pan, D.R. Hu, B.Y. Chu, Y. Qu, Z. Y. Qian, Genetically programmable cell membrane-camouflaged nanoparticles for targeted combination therapy of colorectal cancer, Signal Transduct. Targeted Ther. 9 (2024) 158, https://doi.org/10.1038/s41392-024-01859-4.
[14] Y. Hao, Y.W. Chen, X.L. He, R.X. Han, C.L. Yang, T.L. Liu, Y. Yang, Q.Y. Liu, Z. Y. Qian, RGD peptide modified platinum nanozyme Co-loaded glutathione-responsive prodrug nanoparticles for enhanced chemo-photodynamic bladder cancer therapy, Biomaterials 293 (2023) 121975, https://doi.org/10.1016/j.biomaterials.2022.121975.
[15] S.H. Wang, K.M. Chen, K. Chen, C. Xu, P.W. Ma, G.H. Dang, Y.Q. Yang, Q. Lei, H. Y. Huang, Y. Yu, Y. Fang, Q.Y. Tang, N. Jiang, H.L. Miao, F.A. Liu, X. Zhao, N. Li, Nanoparticle-based medicines in clinical cancer therapy, Nano Today 45 (2022) 1015122, https://doi.org/10.1016/j.nantod.2022.101512.
[16] N. Khaiwa, N.R. Maarouf, M.H. Darwish, D.W.M. Alhamad, A. Sebastian, M. Hamad, H.A. Omar, G. Orive, T.H. Al-Tel, Camptothecin's journey from discovery to WHO Essential Medicine: fifty years of promise, Eur. J. Med. Chem. 223 (2021) 113639, https://doi.org/10.1016/j.ejmech.2021.113639.
[17] Y. Yang, D.R. Hu, Y. Lu, B.Y. Chu, X.L. He, Y. Chen, Y. Xiao, C.L. Yang, K. Zhou, L. P. Yuan, Z.Y. Qian, Tumor-targeted/reduction-triggered composite multifunctional nanoparticles for breast cancer chemo-photothermal combinational therapy, Acta Pharm. Sin. B 12 (2022) 2710–2730, https://doi.org/10.1016/j.apsb.2021.08.021.
[18] G. Tao, J.Q. Huang, B. Moorthy, C. Wang, M. Hu, S. Gao, R. Ghose, Potential role of drug metabolizing enzymes in chemotherapy-induced gastrointestinal toxicity and hepatotoxicity, Expet Opin. Drug Metabol. Toxicol. 16 (2020) 1109–1124, https://doi.org/10.1080/17425255.2020.1815705.
[19] Q.Y. Liu, Y. Lu, Y. Xiao, L.P. Yuan, D.R. Hu, Y. Hao, R.X. Han, J.R. Peng, Z.Y. Qian, Effects of docetaxel injection and docetaxel micelles on the intestinal barrier and intestinal microbiota, Adv. Sci. 8 (2021) e2102952, https://doi.org/10.1002/advs.202102952.
[20] T. Hueso, K. Ekpe, C. Mayeur, A. Gatse, M.J.C. Curt, G. Gricourt, C. Rodriguez, C. Burdet, G. Ulmann, C. Neut, S.E. Amini, P. Lepage, B. Raynard, C. Willekens, J. B. Micol, S. De Botton, I. Yakoub-Agha, F. Gottrand, J.L. Desseyn, M. Thomas, P. L. Woerther, D. Seguy, Impact and consequences of intensive chemotherapy on intestinal barrier and microbiota in acute myeloid leukemia: the role of mucosal strengthening, Gut Microb. 12 (2020) 1800897, https://doi.org/10.1080/19490976.2020.1800897.
[21] J. Tulkens, G. Vergauwen, J. Van Deun, E. Geeurickx, B. Dhondt, L. Lippens, M. A. De Scheerder, I. Miinalainen, P. Rappu, B.G. De Geest, K. Vandecasteele, D. Laukens, L. Vandekerckhove, H. Denys, J. Vandesompele, O. De Wever, A. Hendrix, Increased levels of systemic LPS-positive bacterial extracellular vesicles in patients with intestinal barrier dysfunction, Gut 69 (2020) 191–193, https://doi.org/10.1136/gutjnl-2018-317726.
[22] C. Chelakkot, J. Ghim, S.H. Ryu, Mechanisms regulating intestinal barrier integrity and its pathological implications, Exp. Mol. Med. 50 (2018) 103, https://doi.org/10.1038/s12276-018-0126-x.
[23] X.Y. Wang, S.S. Lin, L. Wang, Z.P. Cao, M.M. Zhang, Y.F. Zhang, R. Liu, J.Y. Liu, Versatility of bacterial outer membrane vesicles in regulating intestinal homeostasis, Sci. Adv. 9 (2023) eade5079, https://doi.org/10.1126/sciadv.ade5079.
[24] Z. Zhao, J.W. Ning, X.Q. Bao, M.Y. Shang, J.W. Ma, G. Li, D. Zhang, Fecal microbiota transplantation protects rotenone-induced Parkinson's disease mice via suppressing inflammation mediated by the lipopolysaccharide-TLR4 signaling pathway through the microbiota-gut-brain axis, Microbiome 9 (2021) 226, https://doi.org/10.1186/s40168-021-01107-9.
[25] H.R. Wardill, J.M. Bowen, N. Al-Dasooqi, M. Sultani, E. Bateman, R. Stansborough, J. Shirren, R.J. Gibson, Irinotecan disrupts tight junction proteins within the gut: implications for chemotherapy-induced gut toxicity, Cancer Biol. Ther. 15 (2014) 236–244, https://doi.org/10.4161/cbt.27222.
[26] H.R. Wardill, J.M. Bowen, Chemotherapy-induced mucosal barrier dysfunction: an updated review on the role of intestinal tight junctions, Curr. Opin. Support. Palliat. Care 7 (2013) 155–161, https://doi.org/10.1097/SPC.0b013e32835f3e8c.
[27] Y. Kawasaki, K. Kakimoto, Y. Tanaka, H. Shimizu, K. Nishida, K. Numa, N. Kinoshita, Y. Tatsumi, K. Nakazawa, R. Koshiba, Y. Hirata, K. Ota, N. Sakiyama, T. Terazawa, T. Takeuchi, T. Miyazaki, M. Goto, H. Yokota, Y. Makizaki, Y. Tanaka, S. Nakajima, H. Ohno, K. Higuchi, S. Nakamura, H. Nishikawa, Relationship between chemotherapy-induced diarrhea and intestinal microbiome composition, Digestion 104 (2023) 357–369, https://doi.org/10.1159/000528282.
[28] J. Hu, J.W. Chen, X.J. Xu, Q.L. Hou, J. Ren, X.H. Yan, Gut microbiota-derived 3-phenylpropionic acid promotes intestinal epithelial barrier function via AhR signaling, Microbiome 11 (2023) 102, https://doi.org/10.1186/s40168-023-01576-0.
[29] J.L. Alexander, I.D. Wilson, J. Teare, J.R. Marchesi, J.K. Nicholson, J.M. Kinross, Gut microbiota modulation of chemotherapy efficacy and toxicity, Nat. Rev. Gastroenterol. Hepatol. 14 (2017) 356–365, https://doi.org/10.1038/nrgastro.2017.20.
[30] A.M. Stringer, R.J. Gibson, J.M. Bowen, D.M.K. Keefe, Chemotherapy-induced modifications to gastrointestinal microflora: evidence and implications of change, Curr. Drug Metabol. 10 (2009) 79–83, https://doi.org/10.2174/138920009787048419.
[31] H.R. Wang, M.S. Geier, G.S. Howarth, Prebiotics: a potential treatment strategy for the chemotherapy-damaged gut? Crit. Rev. Food Sci. Nutr. 56 (2016) 946–956, https://doi.org/10.1080/10408398.2012.741082.
[32] A.M. Seekatz, C.M. Theriot, C.T. Molloy, K.L. Wozniak, I.L. Bergin, V.B. Young, Fecal microbiota transplantation eliminates Clostridium difficile in a murine model of relapsing disease, Infect. Immun. 83 (2015) 3838–3846, https://doi.org/10.1128/IAI.00459-15.
[33] D.R. Hu, L. Zhong, M.Y. Wang, H.H. Li, Y. Qu, Q.Y. Liu, R.X. Han, L.P. Yuan, K. Shi, J.R. Peng, Z.Y. Qian, Perfluorocarbon-loaded and redox-activatable photosensitizing agent with oxygen supply for enhancement of fluorescence/photoacoustic imaging guided tumor photodynamic therapy, Adv. Funct. Mater. 29 (2019) 1806199, https://doi.org/10.1002/adfm.201806199.
[34] W. Zhang, S.L. Hu, J.J. Yin, W.W. He, W. Lu, M. Ma, N. Gu, Y. Zhang, Prussian blue nanoparticles as multienzyme mimetics and reactive oxygen species scavengers, J. Am. Chem. Soc. 138 (2016) 5860–5865, https://doi.org/10.1021/jacs.5b12070.
[35] M. Li, D. Zhao, J.Q. Yan, X.H. Fu, F.S. Li, G.C. Liu, Y.J. Fan, Y. Liang, X.D. Zhang, A redox-triggered autophagy-induced nanoplatform with PD-L1 inhibition for enhancing combined chemo-immunotherapy, ACS Nano 18 (2024) 12870–12884, https://doi.org/10.1021/acsnano.4c00227.
[36] M.M. Chen, D.P. Liu, F.S. Liu, Y.N. Wu, X.J. Peng, F.L. Song, Recent advances of redox-responsive nanoplatforms for tumor theranostics, J. Contr. Release 332 (2021) 269–284, https://doi.org/10.1016/j.jconrel.2021.02.030.
[37] Q.H. Liu, L.X. He, S.Q. Li, F.Y. Li, G.Z. Deng, X.J. Huang, M.W. Yang, Y.Y. Xiao, X. F. Chen, Y. Ouyang, J.X. Chen, X.X. Wu, X. Wang, L.B. Song, C.Y. Lin, HOMER3 facilitates growth factor-mediated β-Catenin tyrosine phosphorylation and activation to promote metastasis in triple negative breast cancer, J. Hematol. Oncol. 14 (2021) 6, https://doi.org/10.1186/s13045-020-01021-x.
[38] A. Horowitz, S.D. Chanez-Paredes, X. Haest, J.R. Turner, Paracellular permeability and tight junction regulation in gut health and disease, Nat. Rev. Gastroenterol. Hepatol. 20 (2023) 417–432, https://doi.org/10.1038/s41575-023-00766-3.
[39] W. Turpin, S.H. Lee, J.A.R. Garay, K.L. Madsen, J.B. Meddings, L. Bedrani, N. Power, O. Espin-Garcia, W. Xu, M.I. Smith, A.M. Griffiths, P. Moayyedi, D. Turner, E.G. Seidman, A.H. Steinhart, J.K. Marshall, K. Jacobson, D. Mack, H. Huynh, C.N. Bernstein, A.D. Paterson, Increased intestinal permeability is associated with later development of crohn's disease, Gastroenterology 159 (2020) 2092–2100.e5, https://doi.org/10.1053/j.gastro.2020.08.005.
[40] M.J. Ratain, I.F. Tannock, A.S. Lichter, Dose optimization of sotorasib: is the US food and drug administration sending a message? J. Clin. Oncol. 39 (2021) 3423–3426, https://doi.org/10.1200/JCO.21.01371.
[41] B.D. Wallace, H.W. Wang, K.T. Lane, J.E. Scott, J. Orans, J.S. Koo, M. Venkatesh, C. Jobin, L.A. Yeh, S. Mani, M.R. Redinbo, Alleviating cancer drug toxicity by inhibiting a bacterial enzyme, Science 330 (2010) 831–835, https://doi.org/10.1126/science.1191175.
[42] M. Neunlist, F. Toumi, T. Oreschkova, M. Denis, J. Leborgne, C.L. Laboisse, J. P. Galmiche, A. Jarry, Human ENS regulates the intestinal epithelial barrier permeability and a tight junction-associated protein ZO-1 via VIPergic pathways, Am. J. Physiol. Gastrointest. Liver Physiol. 285 (2003) G1028–G1036, https://doi.org/10.1152/ajpgi.00066.2003.
[43] T. Kucharzik, S.V. Walsh, J. Chen, C.A. Parkos, A. Nusrat, Neutrophil transmigration in inflammatory bowel disease is associated with differential expression of epithelial intercellular junction proteins, Am. J. Pathol. 159 (2001) 2001–2009, https://doi.org/10.1016/S0002-9440(10)63051-9.
[44] L. Shen, C.R. Weber, D.R. Raleigh, D. Yu, J.R. Turner, Tight junction pore and leak pathways: a dynamic duo, Annu. Rev. Physiol. 73 (2011) 283–309, https://doi.org/10.1146/annurev-physiol-012110-142150.
[45] Q.Y. Liu, Y. Yang, M. Pan, F. Yang, Y. Yu, Z.Y. Qian, Role of the gut microbiota in tumorigenesis and treatment, Theranostics 14 (2024) 2304–2328, https://doi.org/10.7150/thno.91700.
[46] V. Gopalakrishnan, C.N. Spencer, L. Nezi, A. Reuben, M.C. Andrews, T. V. Karpinets, P.A. Prieto, D. Vicente, K. Hoffman, S.C. Wei, A.P. Cogdill, L. Zhao, C. W. Hudgens, D.S. Hutchinson, T. Manzo, M.P. de Macedo, T. Cotechini, T. Kumar, W.S. Chen, S.M. Reddy, S.R. Sloane, J. Galloway-Pena, H. Jiang, P.L. Chen, E. J. Shpall, K. Rezvani, A.M. Alousi, R.F. Chemaly, S. Shelburne, L.M. Vence, P. C. Okhuysen, V.B. Jensen, A.G. Swennes, F. McAllister, E.M.R. Sanchez, Y. Zhang, E. Le Chatelier, L. Zitvogel, N. Pons, J.L. Austin-Breneman, L.E. Haydu, E. M. Burton, J.M. Gardner, E. Sirmans, J. Hu, A.J. Lazar, T. Tsujikawa, A. Diab, H. Tawbi, I.C. Glitza, W.J. Hwu, S.P. Patel, S.E. Woodman, R.N. Amaria, M. A. Davies, J.E. Gershenwald, P. Hwu, J.E. Lee, J. Zhang, L.M. Coussens, Z. A. Cooper, P.A. Futreal, C.R. Daniel, N.J. Ajami, J.F. Petrosino, M.T. Tetzlaff, P. Sharma, J.P. Allison, R.R. Jenq, J.A. Wargo, Gut microbiome modulates response to anti-PD-1 immunotherapy in melanoma patients, Science 359 (2018) 97–103, https://doi.org/10.1126/science.aan4236.
[47] Z.T. Yu, D.G. Li, H.X. Sun, Herba Origani alleviated DSS-induced ulcerative colitis in mice through remolding gut microbiota to regulate bile acid and short-chain fatty acid metabolisms, Biomed. Pharmacother. 161 (2023) 114409, https://doi.org/10.1016/j.biopha.2023.114409.

[48] P.P. Feng, Z.P. Cao, X.Y. Wang, J.J. Li, J.Y. Liu, On-demand bacterial reactivation by restraining within a triggerable nanocoating, Adv. Mater. 32 (2020) e2002406, https://doi.org/10.1002/adma.202002406.
[49] W.J.Y. Chee, S.Y. Chew, L.T.L. Than, Vaginal microbiota and the potential of Lactobacillus derivatives in maintaining vaginal health, Microb. Cell Factories 19 (2020) 203, https://doi.org/10.1186/s12934-020-01464-4.
[50] T.F. Du, A.H. Lei, N.Y. Zhang, C.M. Zhu, The beneficial role of probiotic lactobacillus in respiratory diseases, Front. Immunol. 13 (2022) 908010, https://doi.org/10.3389/fimmu.2022.908010.
[51] M.E. Sanders, D.J. Merenstein, G. Reid, G.R. Gibson, R.A. Rastall, Probiotics and prebiotics in intestinal health and disease: from biology to the clinic, Nat. Rev. Gastroenterol. Hepatol. 16 (2019) 605–616, https://doi.org/10.1038/s41575-019-0173-3.
[52] M.S. Pereira, M.A. Kriegel, Translocating Lactobacillus torments tumors via tryptophan catabolism, Cell 186 (2023) 1821–1823, https://doi.org/10.1016/j.cell.2023.03.022.
[53] M.J. Bender, A.C. McPherson, C.M. Phelps, S.P. Pandey, C.R. Laughlin, J. H. Shapira, L.M. Sanchez, M. Rana, T.G. Richie, T.S. Mims, A.M. Gocher-Demske, L. Cervantes-Barragan, S.J. Mullett, S.L. Gelhaus, T.C. Bruno, N. Cannon, J. A. McCulloch, D.A.A. Vignali, R. Hinterleitner, A.V. Joglekar, J.F. Pierre, S.T. M. Lee, D. Davar, H.M. Zarour, M. Meisel, Dietary tryptophan metabolite released by intratumoral Lactobacillus reuteri facilitates immune checkpoint inhibitor treatment, Cell 186 (2023) 846–1862.e26, https://doi.org/10.1016/j.cell.2023.03.011.
[54] H.N. Bell, R.J. Rebernick, J. Goyert, R. Singhal, M. Kuljanin, S.A. Kerk, W. Huang, N.K. Das, A. Andren, S. Solanki, S.L. Miller, P.K. Todd, E.R. Fearon, C.A. Lyssiotis, S.P. Gygi, J.D. Mancias, Y.M. Shah, Reuterin in the healthy gut microbiome suppresses colorectal cancer growth through altering redox balance, Cancer Cell 14 (2022) 185–200.e6, https://doi.org/10.1016/j.ccell.2021.12.001.
[55] V. Liévin-Le Moal, A.L. Servin, Anti-infective activities of lactobacillus strains in the human intestinal microbiota: from probiotics to gastrointestinal anti-infectious biotherapeutic agents, Clin. Microbiol. Rev. 27 (2014) 167–199, https://doi.org/10.1128/CMR.00080-13.
[56] J.J. Hou, X. Wang, Y.M. Wang, B.M. Wang, Interplay between gut microbiota and bile acids in diarrhoea-predominant irritable bowel syndrome: a review, Crit. Rev. Microbiol. 48 (2022) 696–713, https://doi.org/10.1080/1040841X.2021.2018401.
[57] A.G. Cheng, P.Y. Ho, A. Aranda-Díaz, S. Jain, F.Q.B. Yu, X.D. Meng, M. Wang, M. Iakiviak, K. Nagashima, A.S. Zhao, P. Murugkar, A. Patil, K. Atabakhsh, A. Weakley, J. Yan, A.R. Brumbaugh, S. Higginbottom, A. Dimas, A.L. Shiver, A. Deutschbauer, N. Neff, J.L. Sonnenburg, K.C. Huang, M.A. Fischbach, Design, construction, and in vivo augmentation of a complex gut microbiome, Cell 185 (2022) 3617–3636.e19, https://doi.org/10.1016/j.cell.2022.08.003.
[58] L.T. Wang, H.P. Kuo, Y.C. Wu, C.J. Tai, F.L. Lee, Lactobacillus taiwanensis sp. nov., isolated from silage, Int. J. Syst. Evol. Microbiol. 59 (2009) 2064–2068, https://doi.org/10.1099/ijs.0.006783-0.
[59] S. Maehana, H. Kitasato, M. Suzuki, Genome sequence of acinetobacter towneri strain DSM 16313, previously known as the proposed type strain of acinetobacter seohaensis, Microbiol Resour Announc 10 (2021) e0069021, https://doi.org/10.1128/MRA.00690-21.
[60] J. Sato, A. Kanazawa, F. Ikeda, T. Yoshihara, H. Goto, H. Abe, K. Komiya, M. Kawaguchi, T. Shimizu, T. Ogihara, Y. Tamura, Y. Sakurai, R. Yamamoto, T. Mita, Y. Fujitani, H. Fukuda, K. Nomoto, T. Takahashi, T. Asahara, T. Hirose, S. Nagata, Y. Yamashiro, H. Watada, Gut dysbiosis and detection of "ive gut bacteria" in blood of Japanese patients with type 2 diabetes, Diabetes Care 37 (2014) 2343–2350, https://doi.org/10.2337/dc13-2817.
[61] G.P. Nickolson, N.M. Balasjin, C.W. Marshall, Draft genome sequence of Staphylococcus succinus strain GN1, isolated from a basement floor in Milwaukee, WI, Microbiol Resour Announc 10 (2021) e0058021, https://doi.org/10.1128/MRA.00580-21.
[62] A.R. Bujold, A.E. Shure, R. Liu, A.M. Kropinski, J.I. MacInnes, Investigation of putative invasion determinants of Actinobacillus species using comparative genomics, Genomics 111 (2019) 59–66, https://doi.org/10.1016/j.ygeno.2018.01.001.
[63] N. Yang, W.Y. Xiao, X.J. Song, W.J. Wang, X.C. Dong, Recent advances in tumor microenvironment hydrogen peroxide-responsive materials for cancer photodynamic therapy, Nano-Micro Lett. 12 (2020) 15, https://doi.org/10.1007/s40820-019-0347-0.
[64] Y. Zhu, D. Jin, M.M. Liu, Y. Dai, L. Li, X.W. Zheng, L.L. Wang, A.Z. Shen, J.N. Yu, S. S. Wu, Y. Wu, K. Zhong, J.J. Cheng, Y.Z. Liu, Oxygen self-supply engineering-ferritin for the relief of hypoxia in tumors and the enhancement of photodynamic therapy efficacy, Small 18 (2022) e2200116, https://doi.org/10.1002/smll.202200116.
[65] W.M. Zhang, D. Ma, J.X. Du, Prussian blue nanoparticles as peroxidase mimetics for sensitive colorimetric detection of hydrogen peroxide and glucose, Talanta 120 (2014) 362–367, https://doi.org/10.1016/j.talanta.2013.12.028.
[66] Y. Litvak, M.X. Byndloss, A.J. Bäumler, Colonocyte metabolism shapes the gut microbiota, Science 362 (2018) eaat9076, https://doi.org/10.1126/science.aat9076.
[67] J.R. Peng, M.L. Dong, B. Ran, W.T. Li, Y. Hao, Q. Yang, L.W. Tan, K. Shi, Z.Y. Qian, "One-for-All"-Type, biodegradable prussian blue/manganese dioxide hybrid nanocrystal for trimodal imaging-guided photothermal therapy and oxygen regulation of breast cancer, ACS Appl. Mater. Interfaces 9 (2017) 13875–13886, https://doi.org/10.1021/acsami.7b01365.